Histone H3.3 beyond cancer: Germline mutations in Histone 3 Family 3A and 3B cause a previously unidentified neurodegenerative disorder in 46 patients

Laura Bryant, Dong Li, Samuel G Cox, Dylan Marchione, Evan F Joiner, Khadija Wilson, Kevin Janssen, Pearl Lee, Michael E March, Divya Nair, et al.

GENETICS

Histone H3.3 beyond cancer: Germline mutations in *Histone 3 Family 3A and 3B* cause a previously unidentified neurodegenerative disorder in 46 patients

Laura Bryant[1]*, Dong Li[1]*, Samuel G. Cox[2], Dylan Marchione[3], Evan F. Joiner[4], Khadija Wilson[3], Kevin Janssen[3], Pearl Lee[5], Michael E. March[1], Divya Nair[1], Elliott Sherr[6], Brieana Fregeau[6], Klaas J. Wierenga[7], Alexandrea Wadley[7], Grazia M. S. Mancini[8], Nina Powell-Hamilton[9], Jiddeke van de Kamp[10], Theresa Grebe[11], John Dean[12], Alison Ross[12], Heather P. Crawford[13], Zoe Powis[14], Megan T. Cho[15], Marcia C. Willing[16], Linda Manwaring[16], Rachel Schot[8], Caroline Nava[17,18], Alexandra Afenjar[19], Davor Lessel[20,21], Matias Wagner[22,23,24], Thomas Klopstock[25,26,27], Juliane Winkelmann[22,24,27,28], Claudia B. Catarino[25], Kyle Retterer[15], Jane L. Schuette[29], Jeffrey W. Innis[29], Amy Pizzino[30,31], Sabine Lüttgen[32], Jonas Denecke[32], Tim M. Strom[22,24], Kristin G. Monaghan[15]; DDD Study, Zuo-Fei Yuan[3], Holly Dubbs[30,31], Renee Bend[33], Jennifer A. Lee[33], Michael J. Lyons[33], Julia Hoefele[24], Roman Günthner[34,35], Heiko Reutter[36], Boris Keren[18], Kelly Radtke[37], Omar Sherbini[30,31], Cameron Mrokse[37], Katherine L. Helbig[37], Sylvie Odent[38], Benjamin Cogne[39,40], Sandra Mercier[39,40], Stephane Bezieau[39,40], Thomas Besnard[39,40], Sebastien Kury[39,40], Richard Redon[40], Karit Reinson[41,42], Monica H. Wojcik[43,44], Katrin Õunap[41,42], Pilvi Ilves[45], A. Micheil Innes[46], Kristin D. Kernohan[47,48]; Care4Rare Canada Consortium, Gregory Costain[49], M. Stephen Meyn[49,50], David Chitayat[49,51], Elaine Zackai[52], Anna Lehman[53], Hilary Kitson[54]; CAUSES Study, Martin G. Martin[55,56], Julian A. Martinez-Agosto[57,58]; Undiagnosed Diseases Network, Stan F. Nelson[57,59], Christina G. S. Palmer[57,60], Jeanette C. Papp[57], Neil H. Parker[61], Janet S. Sinsheimer[62], Eric Vilain[63], Jijun Wan[57], Amanda J. Yoon[57], Allison Zheng[57], Elise Brimble[64], Giovanni Battista Ferrero[65], Francesca Clementina Radio[66], Diana Carli[65], Sabina Barresi[66], Alfredo Brusco[67], Marco Tartaglia[66], Jennifer Muncy Thomas[68], Luis Umana[69], Marjan M. Weiss[10], Garrett Gotway[69], K. E. Stuurman[8], Michelle L. Thompson[70], Kirsty McWalter[15], Constance T. R. M. Stumpel[71], Servi J. C. Stevens[71], Alexander P. A. Stegmann[71], Kristian Tveten[72], Arve Vøllo[73], Trine Prescott[72], Christina Fagerberg[74], Lone Walentin Laulund[75], Martin J. Larsen[74], Melissa Byler[76], Robert Roger Lebel[76], Anna C. Hurst[77], Joy Dean[77], Samantha A. Schrier Vergano[78], Jennifer Norman[79], Saadet Mercimek-Andrews[49], Juanita Neira[80], Margot I. Van Allen[53,81], Nicola Longo[82], Elizabeth Sellars[83], Raymond J. Louie[33], Sara S. Cathey[33], Elly Brokamp[84], Delphine Heron[18], Molly Snyder[85], Adeline Vanderver[30,31], Celeste Simon[4], Xavier de la Cruz[86,87], Natália Padilla[86], J. Gage Crump[2], Wendy Chung[88], Benjamin Garcia[2,3], Hakon H. Hakonarson[1], Elizabeth J. Bhoj[1†]

Although somatic mutations in Histone 3.3 (H3.3) are well-studied drivers of oncogenesis, the role of germline mutations remains unreported. We analyze 46 patients bearing de novo germline mutations in histone 3 family 3A (*H3F3A*) or *H3F3B* with progressive neurologic dysfunction and congenital anomalies without malignancies. Molecular modeling of all 37 variants demonstrated clear disruptions in interactions with DNA, other histones, and histone chaperone proteins. Patient histone posttranslational modifications (PTMs) analysis revealed notably aberrant local PTM patterns distinct from the somatic lysine mutations that cause global PTM dysregulation. RNA sequencing on patient cells demonstrated up-regulated gene expression related to mitosis and cell division, and cellular assays confirmed an increased proliferative capacity. A zebrafish model showed craniofacial anomalies and a defect in Foxd3-derived glia. These data suggest that the mechanism of germline mutations are distinct from cancer-associated somatic histone mutations but may converge on control of cell proliferation.

INTRODUCTION

The study of histones and their role in epigenetics is a rapidly expanding field. Histones are nuclear proteins that associate with DNA to facilitate packaging into condensed chromatin. Histones are dynamically decorated with posttranslational modifications (PTMs), which regulate these processes as DNA repair, gene expression, mitosis, and meiosis. Dysregulation of PTMs leads to cancer, neurodevelopmental syndromes, psychiatric disorders, and even cardiovascular disease (*1*–*4*). The vast array of diseases that stem from histone dysregulation makes understanding histone biology vital to understanding the pathophysiology of many diseases and developing treatments. Histones are highly evolutionarily conserved, and only a few germline disease-causing variants in the histones themselves have been found (*5*). Rather, most disease-causing variants affecting

histone regulation are found in histone-modifying proteins or histone chaperones. Somatic mutations in histone H3.3 (H3.3), encoded by both *H3F3A* and *H3F3B*, have recently been identified in pediatric glia and other tumors. This discovery revolutionized the field of epigenetic changes in tumors and how they lead to cancer progression (*6*). There has been one case report suggesting a relationship between a neurodevelopmental syndrome and *H3F3A*, but no additional patients or functional data have been published previously (*7*). Studying how histone mutations cause disease can provide the key to understanding how mutations in the histone network lead to disease.

Histone 3 family 3 (H3F3) histones (H3.3) mark active genes, maintain epigenetic memory, and maintain heterochromatin and telomeric integrity. Every nucleosome contains a version of H3. H3.1 and H3.2 are canonical histones that are replication dependent and, therefore, added to chromatin only during DNA replication. H3.3, however, is a replication-independent variant, which differs from the canonical H3.1 and H3.2 by only five and four amino acids, respectively (*8*). *H3F3A* and *H3F3B* code for an identical protein product, H3.3, a 135–amino acid protein (after cleavage of the first methionine) with a histone tail, four α helices, and two loop domains. These genes, however, contain different regulatory and coding sequences, which lead to different expression patterns and levels for *H3F3A* and *H3F3B*. Both *H3F3B* and *H3F3A* are expressed ubiquitously, during development and throughout life, with relatively high levels of expression in the brain, testes, ovaries, and uterus (*9*).

Because of the biologic importance of *H3F3A* and *H3F3B*, their orthologs have been studied extensively in multiple model organisms. When both *H3f3a* and *H3f3b* are knocked out in mice, it causes embryonic lethality at embryonic day 6.5, and reduced expression leads to sterility, growth retardation, and increased neonatal lethality

[1]Center for Applied Genomics, Children's Hospital of Philadelphia, Philadelphia, PA 19104, USA. [2]Department of Stem Cell Biology and Regenerative Medicine, Keck School of Medicine, University of Southern California, CA 90033, USA. [3]Epigenetics Institute, Department of Biochemistry and Biophysics, Perelman School of Medicine, University of Pennsylvania, Philadelphia, PA 19104, USA. [4]Vagelos College of Physicians and Surgeons, Columbia University, New York, NY 10032, USA. [5]Abramson Family Cancer Research Institute, Perelman School of Medicine, University of Pennsylvania, Philadelphia, PA 19104, USA. [6]Department of Neurology, University of California, San Francisco, San Francisco, CA 94158, USA. [7]Department of Clinical Genomics, Mayo Clinic Florida, Jacksonville, FL 32224, USA. [8]Department of Clinical Genetics, Erasmus University Medical Center, 3015 CN Rotterdam, Netherlands. [9]Department of Medical Genetics, Alfred I. duPont Hospital for Children, Wilmington, DE 19810, USA. [10]Department of Clinical Genetics, VU Medical Center, Amsterdam, Netherlands. [11]Division of Genetics and Metabolism, Phoenix Children's Hospital, Phoenix, AZ 85016, USA. [12]Department of Medical Genetics, Aberdeen Royal Infirmary, Aberdeen, Scotland, UK. [13]Clinical and Metabolic Genetics, Cook Children's Medical Center, Fort Worth, TX 76104, USA. [14]Department of Emerging Genetic Medicine, Ambry Genetics, Aliso Viejo, CA 92656, USA. [15]GeneDx, 207 Perry Parkway, Gaithersburg, MD 20877, USA. [16]Division of Genetics and Genomic Medicine, Department of Pediatrics, Washington University in St. Louis, School of Medicine, St. Louis, MO 63110, USA. [17]Sorbonne Universités, UPMC Univ Paris 06, UMR S 1127, Inserm U 1127, CNRS UMR 7225, ICM, Paris, France. [18]AP-HP, Hôpital de la Pitié-Salpêtrière, Département de Génétique, F-75013 Paris, France. [19]Service de génétique, CRMR des malformations et maladies congénitales du cervelet et CRMR déficience intellectuelle, hôpital Trousseau, AP-HP, France. [20]Institute of Human Genetics, University Medical Center Hamburg-Eppendorf, 20246 Hamburg, Germany. [21]Undiagnosed Disease Program at the University Medical Center Hamburg-Eppendorf (UDP-UKE), Martinistrasse 52, 20246 Hamburg, Germany. [22]Institut für Neurogenomik, Helmholtz Zentrum München, Munich, Germany. [23]Institut für Humangenetik, Helmholtz Zentrum München, Munich, Germany. [24]Institut für Humangenetik, Technische Universität München, Munich, Germany. [25]Friedrich-Baur-Institute, Department of Neurology, Ludwig-Maximilians University, Ziemssenstr. 1a, 80336 Munich, Germany. [26]German Center for Neurodegenerative Diseases (DZNE), Munich, Germany. [27]Munich Cluster for Systems Neurology, SyNergy, Munich, Germany. [28]Klinik und Poliklinik für Neurologie, Klinikum rechts der Isar, Technische Universität München, Munich, Germany. [29]Division of Genetics, Metabolism, and Genomic Medicine, Department of Pediatrics and Communicable Diseases, University of Michigan, Ann Arbor, MI 48109, USA. [30]Division of Neurology, Children's Hospital of Philadelphia, Philadelphia, PA 19104, USA. [31]Perelman School of Medicine, University of Pennsylvania, Philadelphia, PA 19103, USA. [32]Department of Pediatrics, University Medical Center Eppendorf, 20246 Hamburg, Germany. [33]Greenwood Genetic Center, Greenwood, SC 29646, USA. [34]Department of Nephrology, Klinikum Rechts der Isar, Technical University Munich, Munich, Germany. [35]Institute of Human Genetics, Klinikum Rechts der Isar, Technical University Munich, Munich, Germany. [36]Department of Neonatology and Pediatric Intensive Care, Children's Hospital, University Hospital Bonn & Institute of Human Genetics, University Hospital Bonn, Bonn, Germany. [37]Department of Clinical Genomics, Ambry Genetics, Aliso Viejo, CA 92656, USA. [38]CHU Rennes, Service de Génétique Clinique, CNRS UMR6290, University Rennes1, Rennes, France. [39]CHU Nantes, Service de Génétique Médicale, 9 quai Moncousu, 44093 Nantes, France. [40]INSERM, CNRS, UNIV Nantes, CHU Nantes, l'institut du thorax, 44007 Nantes, France. [41]Department of Clinical Genetics, United Laboratories, Tartu University Hospital, Tartu, Estonia. [42]Institute of Clinical Medicine, University of Tartu, Tartu, Estonia. [43]Division of Genetics and Genomics and Division of Newborn Medicine, Department of Medicine, Boston Children's Hospital, Harvard Medical School, Boston, MA 02115, USA. [44]Broad Institute, Cambridge, MA 02142, USA. [45]Radiology Department of Tartu University Hospital and Institute of Clinical Medicine, University of Tartu, Tartu, Estonia. [46]Alberta Children's Hospital Research Institute, Department of Medical Genetics, Cumming School of Medicine, University of Calgary, Calgary, Alberta, Canada. [47]Children's Hospital of Eastern Ontario Research Institute, Ottawa, Ontario K1H8L1, Canada. [48]Newborn Screening Ontario (NSO), Children's Hospital of Eastern Ontario, Ottawa, Ontario, Canada. [49]Division of Clinical and Metabolic Genetics, Department of Pediatrics, University of Toronto, The Hospital for Sick Children, Toronto, Ontario, Canada. [50]The Center for Human Genomics and Precision Medicine, School of Medicine and Public Health, University of Wisconsin – Madison, Madison, Wisconsin 53705, USA. [51]The Prenatal Diagnosis and Medical Genetics Program, Mount Sinai Hospital, Toronto, Ontario, Canada. [52]Division of Human Genetics, Children's Hospital of Philadelphia, Philadelphia, PA 19104, USA. [53]Department of Medical Genetics, University of British Columbia, Vancouver, Canada. [54]Department of Pediatrics, University of British Columbia, Vancouver, Canada. [55]Division of Gastroenterology and Nutrition, Department of Pediatrics, Mattel Children's Hospital, Los Angeles, CA 90095, USA. [56]Eli and Edythe Broad Center of Regenerative Medicine and Stem Cell Research and the David Geffen School of Medicine, UCLA, Los Angeles, CA 90095, USA. [57]Department of Human Genetics, David Geffen School of Medicine, UCLA, Los Angeles, CA 90095, USA. [58]Division of Medical Genetics, Department of Pediatrics, David Geffen School of Medicine, UCLA, Los Angeles, CA 90095, USA. [59]Department of Pathology and Laboratory Medicine, David Geffen School of Medicine, UCLA, Los Angeles, CA 90095, USA. [60]Institute for Society and Genetics, Department of Psychiatry and Biobehavioral Sciences, David Geffen School of Medicine, UCLA, Los Angeles, CA 90095, USA. [61]David Geffen School of Medicine, Los Angeles, CA 90095, USA. [62]Institute for Society and Genetics, Departments of Human Genetics, Biomathematics, and Biostatistics, David Geffen School of Medicine, UCLA, Los Angeles, CA 90095, USA. [63]Center for Genetic Medicine Research, Children's National Medical Center, Washington, DC 20010, USA. [64]Department of Neurology and Neurological Sciences, Stanford Medicine, Stanford, CA 94305, USA. [65]Department of Public Health and Pediatrics, University of Torino, Turin, Italy. [66]Genetics and Rare Diseases Research Division, Ospedale Pediatrico Bambino Gesù, Rome, Italy. [67]Department of Medical Sciences, University of Torino, Turin, Italy. [68]Pediatrics and Neurology and Neurotherapeutics, UT Southwestern Medical Center, Dallas, TX 75390, USA. [69]Genetics and Metabolism, UT Southwestern Medical Center, Dallas, TX 75390, USA. [70]HudsonAlpha Institute for Biotechnology, Huntsville, AL 35806, USA. [71]Department of Clinical Genetics, Maastricht University Medical Center, Maastricht, Netherlands. [72]Department of Medical Genetics, Telemark Hospital Trust, 3710 Skien, Norway. [73]Department of Pediatrics, Hospital of Østfold, 1714 Grålum, Norway. [74]Department of Clinical Genetics, Odense University Hospital, Odense, Denmark. [75]H.C. Andersen Children's Hospital, Odense University Hospital, Odense, Denmark. [76]SUNY Upstate Medical University, Syracuse, NY 13210, USA. [77]University of Alabama at Birmingham, Birmingham, AL 35294, USA. [78]Division of Medical Genetics and Metabolism, Children's Hospital of The King's Daughters, Norfolk VA 23507, USA. [79]INTEGRIS Pediatric Neurology, Oklahoma City, OK 73112, USA. [80]Department of Human Genetics, Emory University, Atlanta, GA 30322, USA. [81]Medical Genetics Programs, Provincial Health Shared Services BC and Vancouver Island Health Shared Services BC, Canada. [82]Division of Medical Genetics, Department of Pediatrics, University of Utah, Salt Lake City, UT 84112, USA. [83]University of Arkansas for Medical Sciences, Little Rock, AR 72701, USA. [84]Vanderbilt University, Nashville, TN 37203, USA. [85]Child Neurology, UT Southwestern Medical Center, Dallas, TX 75390, USA. [86]Vall d'Hebron Institute of Research (VHIR), Universitat Autònoma de Barcelona, Barcelona, Spain. [87]Institució Catalana de Recerca i Estudis Avançats (ICREA), Barcelona, Spain. [88]Departments of Pediatrics and Medicine, Columbia University Irving Medical Center, New York, NY 10032, USA.
*Co-first authors.
†Corresponding author. Email: bhoje@email.chop.edu

(*10*). Disrupting either *His3.3A* or *His3.3B* in *Drosophila* is tolerated; however, disrupting both leads to sterility and increased lethality (*11*). While knockout models have been studied in mice and *Drosophila*, germline missense mutations have not. There have been many studies in yeast that show the lethality of various missense mutations, but it is difficult to infer whether that means missense mutations in humans would also have a profound effect (*12*).

In this work, we have identified a cohort of 46 unrelated patients bearing de novo heterozygous germline missense mutations in *H3F3A* or *H3F3B* with a core phenotype of progressive neurologic dysfunction and congenital anomalies. Notably, although all known H3.3 mutations in humans cause cancer, none of the patients in our cohort have cancer. These mutations are distinct and appear to be acting, although it is a completely different pathogenic mechanism than the cancer-causing mutations. The mutations are spread throughout the coding sequence, and neither the location of the mutation nor whether the mutation is in *H3F3A* or *H3F3B* appears to affect the phenotype. The breadth of these previously unidentified disease-causing mutations in *H3F3A* and *H3F3B* provides evidence for how sensitive the neural-related functions of H3.3 are to small variation.

RESULTS

Patient mutations and phenotype

Our patient cohort consists of 46 unrelated patients bearing de novo germline missense mutations in *H3F3A* or *H3F3B* (Fig. 1). Both *H3F3A* and *H3F3B* code for H3.3. Therefore, a heterozygous mutation in either gene would affect only about 25% of the total H3.3 in the cell, depending on different expression levels from the two genes. None of the patients have malignancies, but they share a phenotype of developmental delay, usually severe and often progressive, with mostly minor congenital anomalies (Table 1). These patients were identified through exome or genome sequencing performed for the indication of neurodevelopmental delays and/or congenital anomalies (Table 1, fig. S1, and table S1). There is substantial phenotypic heterogeneity in the patients, and future individuals are likely to be identified using unbiased molecular testing. Notably, 9 of the 46 patients (21%) have demonstrated clinical neurologic degeneration, which suggests that this may be a progressive disorder. Multiple patients (26% of the cohort) have cortical atrophy on brain magnetic resonance imaging (MRI), even without intractable epilepsy. For example, the oldest patient in this cohort (32 years) developed seizures at the age of 14 years and a progressive spastic paraparesis starting at the age of 29 years.

The severity of the phenotype does not correlate with the location of the mutation or whether the mutation is in *H3F3A* or *H3F3B*. Four unrelated patients have the p.T45I mutation and exhibit the full range of the phenotype severity. The age at sitting for patients with the p.T45I mutation ranges from 8 months to not achieved within 4.5 years. The age at walking was 21 months, 2 years, and 3 years and not achieved at 4.5 years. One exhibited developmental regression, while the other three did not, and only one has seizures. Even the tone abnormalities are inconsistent with three exhibiting hypotonia, while one has hypertonia. This strongly suggests that the variation in phenotype is not due to the location of the mutation but rather due to either modifying alleles or environmental factors.

Five mutations [*H3F3A* (NM_002107.4) p.R17G, p.T45I, p.A114G, p.Q125R, and *H3F3B* (NM_005324.4) p.P121R] were detected in two or more unrelated patients. p.Q125R was found in *H3F3A* in three individuals and in a different individual in *H3F3B*, while p.P121R was found in *H3F3A* in one individual and in *H3F3B* in two other individuals. Notably, in two patients, the mutations (*H3F3A* p.Q125R and p.V117L) were identified only by trio genome sequencing after negative exome sequencing, as the last exon of *H3F3A* is currently not covered by some exome capture kits. We speculate that similar mutations in *H3F3A* may be underdiagnosed in current exome studies. It should be noted for nomenclature consistency purposes that, historically, many publications on H3.3 exclude the initiator methionine in the residue count. In this publication, we will use the traditional histone nomenclature and exclude the first methionine. However, we will include traditional human genetics nomenclature in the clinical table of mutations and include this first residue in the mutation notation.

One mutation in *H3F3B* (p.S146X) is only present in the alternate transcript. It is p.V117V in the canonical transcript. Although the mutation is only in the alternate transcript, the patient phenotype is consistent with the rest of the cohort, and the patient cells have the same phenotype as the other patient cells analyzed. The role of the alternate transcript is currently unknown and requires additional study.

These 37 unique missense mutations in 46 patients are all de novo and, with one exception (*H3F3A* c.362 T > A; p.M120K, 1 incidence), are not found in a large database of 138,632 controls, the Genome Aggregation Database (gnomAD) (*13*). Upon closer view of the raw data for this p.M120K variant, it may be a technical mapping error, as it is only present on one strand and did not meet the previous Exome Aggregation Consortium (ExAC) quality control criteria for reporting. In the general population, both genes have a very low rate of missense variants; the gnomAD missense *Z* score is 3.21 for *H3F3A* and 2.95 for *H3F3B* (>2 is significant) (*13*).

Computational modeling of patient mutations

It is likely that these variants are pathogenic through various different mechanisms, as they are found throughout the entire coding sequence

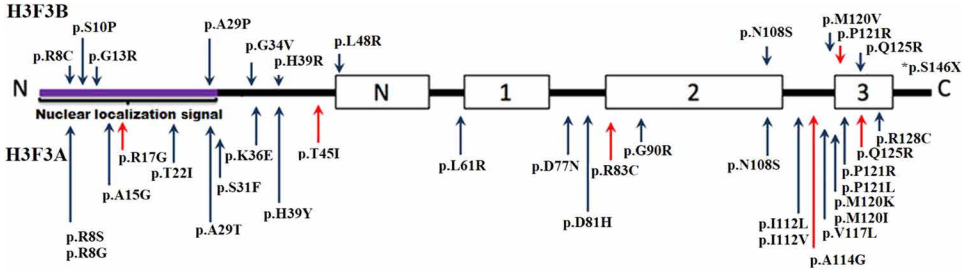

Fig. 1. *H3F3A* mutations (NM_002107.4) and *H3F3B* mutations (NM_005324.4). N, 1, 2, and 3 refer to the N-Helix, Helix-1, Helix-2, and Helix-3 of H3.3, respectively. Upper mutations are encoded by *H3F3B*, and lower mutations are encoded by *H3F3A*. Red arrows indicate mutations found in two or more unrelated patients. A few variants, p.N108S, p.P121R, and p.Q125R, were found in the same position in both *H3F3A* and *H3F3B*. *p.S146X is only present in an *H3F3B* alternate transcript not shown here.

in different domains. To explore these mechanisms further, we used molecular modeling of all 37 of the variants reported here. These 37 variants were mapped to a total of 25 loci distributed over several experimental structures. Eleven locations were in the structure of H3.3 in the nucleosome; at the sequence level, they spread from central positions to near the C-terminal end of H3.3. The remaining 14 locations (as well as H39, which was also present in the nucleosome) were mapped to different complexes between H3.3 and epigenetic regulators. At the sequence level, they concentrated in the N-terminal tail of H3.3.

Table 1. Clinical findings of affected patients. Developmental delay was seen in varying degrees in the majority of patients; hypotonia, poor growth, oculomotor abnormalities, seizures, abnormal skull shape, and microcephaly were also commonly seen in the patients.

33 *H3F3A*/13 *H3F3B*	
25 unique *H3F3A*/12 unique *H3F3B* variants	
3 variants in both *H3F3A* and B	
27 males/19 females	
Ages: 2 months to 32 years; 3 deceased at 2, 10 months, and 2.5 years	
Growth	
Height undergrowth	15/46 (33%)
Height overgrowth	5/46 (11%)
Weight undergrowth	4/37 (11%)
Weight overgrowth	9/37 (27%)
Microcephaly	12/46 (26%)
Development/neurologic	
Achieved independent sitting (range: 6 months to 7 years)	33/45 (73%)
Achieved independent walking (range: 15 months to 8 years)	25/41 (61%)
Spoke at least one word (range: 12 months to 6 years)	16/43 (37%)
Progression of neurologic disease	9/46 (20%)
Brain anomalies on imaging	30/41 (73%)
Cortical atrophy	10/41 (24%)
Seizures	23/46 (50%)
Hypotonia	31/46 (67%)
Spasticity	10/46 (22%)
Contractures	12/46 (22%)
Oculomotor abnormalities	25/46 (54%)
Craniofacial	
High/prominent forehead	14/46 (30%)
Hypertelorism	11/46 (24%)
Craniosynostosis/abnormal head shape (excluding plagiocephaly)	14/46 (30%)
Other	
Atrial septal defect	8/46 (18%)
Skeletal abnormalities	16/46 (35%)
Genital abnormalities	Males 12/27 (44%)
	Females 0/19 (0%)
Chronic constipation	11/45 (24%)

In Fig. 2 (top), we show the location of the variants in the H3.3 structure (for clarity, they are shown only in one H3.3 monomer) and (Fig. 2, bottom) a summary of the amount and type of interatomic contacts at each mutation locus. Together, these data suggest three broad scenarios for the variants' impact. In the first one, variants are likely to disrupt the H3.3-DNA interaction because the native residue is involved in a large number of contacts with the DNA. For instance, this would be the case of p.R83C because the arginine residue penetrates the DNA minor groove. In the second scenario, variants are more likely to disrupt the histone octamer, either because they affect the intramonomer contacts of H3.3 (e.g., p.Q125R) or because they may alter the interaction of H3.3 with other nucleosomal histones (e.g., p.L48R). In the third scenario, the variants disrupt histone-protein binding such as the p.G90R mutation disrupting chaperone binding. In summary, through different mechanisms, the variants in this section are likely to affect the formation, the deposition, or the stability of the nucleosomes containing H3.3 or of the nucleosome pairing. This may result in a generalized loosening of chromatin structure in those processes requiring the incorporation of H3.3 to the nucleosome.

The available complexes between H3.3 and epigenetic regulators (Fig. 3A) involve short stretches of the H3.3 tail bound to sites of different shapes (Fig. 3B). The number of interprotein contacts at the variant locus may vary substantially. For example, p.H39 has 33 and 4 contacts with SETD2 (SET Domain Containing 2, Histone Lysine Methyltransferase) and ZMYND11 (Zinc Finger MYND-Type Containing 11) domains, respectively. We find that residues p.R8, p.S31, p.K36, and p.H39 are involved in more than 10 contacts across epigenetic regulators, suggesting that their mutation may disrupt one or more biologically relevant interactions. For the remaining residues,

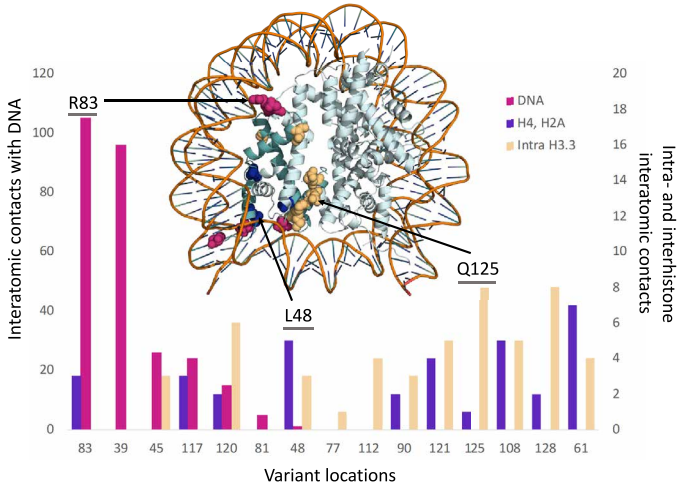

Fig. 2. Variant locations in the nucleosome. At the top of the figure, we show the structure of the nucleosome with the H3.3 variants identified with spheres; the H3.3 monomer carrying them is colored in dark emerald green. The coloring of the variants reflects the predominating interactions at each location: DNA binding (magenta), intramonomer contacts (light orange), and contacts with other histones (dark blue). The same color code is used in the histogram below the structure, where we show the amount of the three interaction types at each location. Note that we use different *y* axis for these interactions: The *y* axis to the left corresponds to the H3.3-DNA binding contacts (magenta bars), and the *y* axis to the right corresponds to the intramonomer (light orange bars) and intermonomer contacts (dark blue bars).

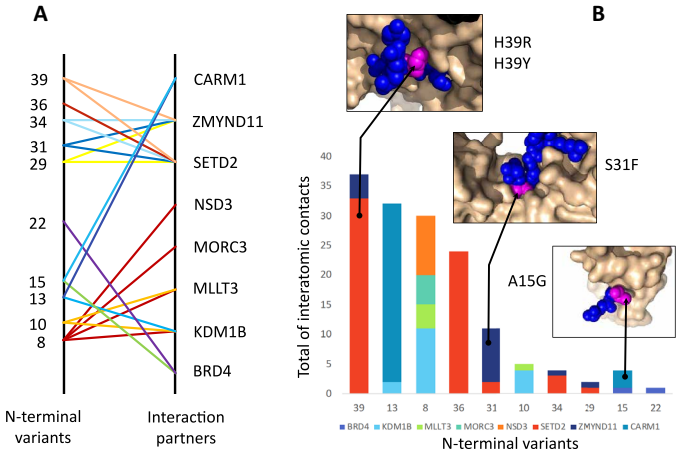

Fig. 3. Variant locations in H3.3-epigenetic regulator complexes. Variant locations could be mapped to the experimental structure of different complexes involving H3.3. In (**A**), we show the variants mapped and the gene names of the H3.3 partners in the corresponding complex. The same color is used for the lines originating in the same variant These complexes include CARM1 (Coactivator Associated Arginine Methyltransferase 1), ZMYND11, SETD2, NSD3 (Histone-lysine N-methyltransferase NSD3), MORC3 (MORC Family CW-Type Zinc Finger 3), MLLT3 (MLLT3 Super Elongation Complex Subunit), KDM1B (Lysine Demethylase 1B), and BRD4. In (**B**), we show the total amount of interatomic interactions at each location, for each H3.3-epigenetic regulator complex. To help interpretation, we give three examples where we can see the histone tail (blue spheres) interacting with its partner (continuous surface in light orange); the histone residue at the variant location is shown in magenta.

the number of interprotein contacts decreases rapidly, limiting our ability to interpret mutation impact. For example, visual analysis of the H3.3-BRD4 (Bromodomain-containing protein 4) complex shows that p.A15 barely participates in the complex between both proteins; contact analysis shows that p.A15 has only one interatomic contact with Brd4. Consequently, we conclude that destabilization of the H3.3-Brd4 complex is an unlikely explanation for pathogenic variants. A general mechanism that may also be valid for variants in the histone tail is that they may disrupt the internucleosome packing, an important interaction in which H3 tails are involved (*14*). In summary, most of the variants in this section are likely to affect the interaction between H3.3 and epigenetic regulators with consequences that will depend on the biological role of each complex, or they may loosen chromatin structure by disrupting internucleosome packing.

Dysregulation of PTMs is distinct for each mutation

To quantify this histone PTM dysregulation, patients' Epstein-Barr virus–transformed lymphoblasts (*H3F3A* p.A15G, *H3F3A* p.R17G, *H3F3A* p.T45I, *H3F3B* p.A29P, and *H3F3B* p.P121R) and primary fibroblasts (*H3F3A* p.R17G, *H3F3A* p.G90R, and *H3F3A* p.T45I) were obtained from patients and age- and ethnicity-matched controls. Histones were extracted and analyzed by nano–liquid chromatography–tandem mass spectrometry (LC-MS/MS) as previously described (*15*). This allowed for a rigorous and robust quantification of histone PTM levels, providing insight into the global epigenetic state in each cell type. For reference, the average of the control lymphoblasts is depicted in Fig. 4A. Notably, analysis of coefficients of variation both within and across patients and controls revealed that the distribution of histone PTM abundances was very similar (Fig. 4B). Although these data show modest changes compared to cells that express p.K27M- or p.K36M-mutant H3.3, which display a near complete loss of di- and trimethylation at K27 or K36, a dominant negative effect cannot be ruled out (*16*).

It was also observed that the overall histone PTM variation was slightly greater in healthy donors than in patients. Nonetheless, some histone PTMs were reproducibly altered when comparing patients to controls (Fig. 4D). Although all patients share a common phenotype of developmental delay, only some of them developed major congenital malformations (i.e., cardiac and cranial anomalies). Further study of the specific local dysregulation during development may lead to insights into the transcriptional control in these processes (i.e., cardiac and cranial development). In general, the magnitude of the changes was modest and may reflect the cell types studied and developmental timing.

The tails of H3.3 and the other H3 histones (1 to 89 amino acids) are identical except for residue 31, where they contain alanine and serine, respectively. Because peptides are generated by cleavage at arginine residues, it is technically impossible to assign PTMs to a specific H3 histone, except in the case of p.A29P. For this case, two PTM abundances (K27 and K36) were compared between (i) protein transcribed from the mutant p.A29P allele from patient cells, (ii) protein transcript from the wild-type (WT) allele from the same patient cells, and (iii) protein transcribed from the two WT alleles from a control (Fig. 4E). These data show notable local deregulation of PTMs on the mutant protein, while the WT protein from the affected patient shows fewer differences from the control. This is a more minor effect than that of published somatic oncogenic mutations; however, the difference neither confirms nor refutes a dominant negative effect (*17*).

Together, these data suggest that the mutant histones can be incorporated into the nucleosome, cause marked local deregulation of chromatin state, and modestly alter the global control of histone modifications. Of greatest interest are the local chromatin changes induced by mutant histone deposition: H3.3 is known to have roles in diverse functions, including gene expression and repression, chromatin stability, DNA damage repair, and differentiation. These mutant proteins and their aberrant PTM states could disrupt any of these processes to lead to the observed phenotype.

Dysregulation of transcripts associated with proliferation and mitosis

To evaluate which biological pathways were differentially perturbed in the patients, we performed RNA sequencing (RNA-seq) on fibroblast cells derived from patients and age- and ethnic-matched controls. All reads were aligned with the STAR (Spliced Transcript Alignment to a Reference) aligner, and Cufflinks was used for performing differential expression analysis. In fibroblast cells (three mutations listed above versus three controls), the H3.3 transcripts (*H3F3A* and *H3F3B*) contribution to total histone H3 expression ranged from 45.1 to 72.6% in cases and 64.1 to 81.7% in controls (table S2). We found 323 genes to be differentially expressed with at least two fold changes in fibroblast cells ($P < 0.05$; table S3). Of these 323 genes, 166 were up-regulated, and 157 were down-regulated in cases. Differentially expressed genes were analyzed through David Functional Annotation Resource, and we found no significant biological signal in the genes with lower expression in cases but showed significant enrichment for up-regulated genes important in mitotic cell cycle process [Benjamini-Hochberg–corrected P ($P_{\text{BH-corrected}}$) = 7.8×10^{-14}], mitotic nuclear division ($P_{\text{BH-corrected}} = 5.8 \times 10^{-10}$), cell division ($P_{\text{BH-corrected}} = 7.5 \times 10^{-10}$), and many other mitosis-related processes (table S4).

To assess whether up-regulation of mitosis-related genes alters cells proliferation, we quantified the cellular proliferation capacity

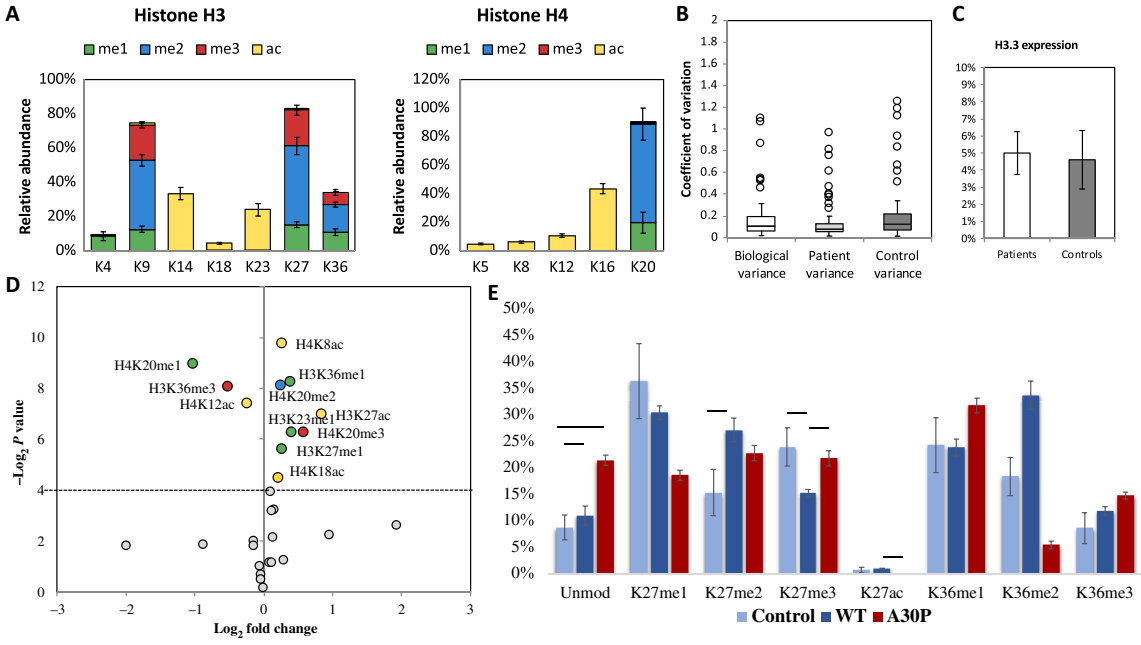

Fig. 4. qMS analysis of patient samples. (**A**) Average profile of PTMs on canonical histones H3 and H4 across control lymphoblasts. Error bars represent SD ($n = 9$ donors; 3 biological replicates each). (**B**) Tukey boxplot depicting the coefficients of variation of 73 modified histone H3 and H4 peptides detected by nano–LC-MS/MS (biological variance: across all 14 donors; patient variance: across five patients; control variance: across nine controls). (**C**) Average histone H3.3 protein abundance (relative to total histone H3) in patient and control lymphoblasts. Error bars represent SD. (**D**) Volcano plot demonstrating significantly altered histone PTMs in patients versus controls. Dotted line represents $P < 0.05$ significance threshold. (**E**) K9 and K14 PTM abundances were compared between (i) protein transcribed from the mutant p.A15G allele from patient cells, (ii) protein transcript from the wild-type (WT) allele from the same patient cells, and (iii) protein transcribed from the WT alleles from a control. Note that the peptide from amino acids 9 to 17 is indistinguishable between canonical H3 and H3.3, so the WT peptide encompasses both. (**F**) A29P is the only mutation occurring on the same peptide that distinguishes H3.3 from H3. PTMs that fall on this peptide are compared across the mutant peptide, the WT peptide from the mutant sample, and the average profile of the peptide from control samples. *$P < 0.05$, **$P < 0.01$, and ***$P < 0.001$. This shows notable local deregulation of PTMs on the mutant peptide. qMS, quantitative mass spectrometry.

of five patient fibroblast lines compared to six age- and sex-matched control fibroblast lines. Patient lines had increased cell proliferation, notably at 72 and 96 hours (Fig. 5A). Furthermore, all five patient lines shared similar viability to the six control lines (Fig. 5B). Cell cycle analyses showed that *H3F3A* p.G90R and *H3F3A* p.T45I had a similar cell cycle profile to the control lines, while *H3F3A* p.R17G showed a decrease in cells in G_1 phase and an increase in cells in S phase compared to all three control lines (Fig. 5C).

Deficit in neural crest–derived cells in a zebrafish model

A dominant zebrafish model (p.D123N) derived from a forward genetic screen has been previously reported with craniofacial abnormalities, which were replicated in our patient cohort (Fig. 6A) (*18*). This heterozygous missense variant replicates the dominant inheritance observed in humans and is only two amino acids away from a mutation identified in an affected patient (p.Q125R). Further investigation of this model also reveals a defect in foxd3-positive neural crest–derived glia, as well as melanocytes and xanthophores (Fig. 6, B to D.) The loss of glial cells may relate to the hypomyelination phenotype that is noted on the brain MRIs of over one-third of the H3.3 cohort as glial cells are the cell type responsible for myelination.

DISCUSSION

The discovery of missense mutations in H3.3 that cause a neurodevelopmental disorder, but not cancer, has profound implications for future research in histone biology. Until now, H3.3 mutations have only been directly linked to cancer (*6*). These specific mutations that cause a neurodevelopmental phenotype are distinct from the ones that cause cancer. The cancer mutations are mostly in lysines in the histone tail, while the only lysine mutation in our cohort is p.K36E. When this lysine-36 is mutated in cancer, it is mutated to methionine and not glutamate (*19*). The patient with the p.K36E mutation was 32 years old when he was last evaluated and still had no signs of cancer, suggesting that the p.K36E mutation does not lead to a strongly increased risk of malignancy. The only other variant in our cohort that is similar to a cancer-linked variant is the p.G34V mutation in *H3F3B*. This p.G34V variant in *H3F3A* has been shown to cause cancer only when combined with mutations in ATRX/DAXX (ATRX Chromatin Remodeler/Death Domain Associated Protein) and TP53 (TAR-DNA binding protein-43) (*19*). Understanding why the somatic p.G34V variant causes cancer, but germline variants cause a neurodevelopmental phenotype, is currently unknown and requires further study.

Notably, although the mutations are spread throughout the coding sequence, they all converge on a similar phenotype. Each mutation affects different specific interactions but converge on the same phenotype. This suggests that the phenotype is due to dysregulation of H3.3 in general and not limited to a single mechanism. Molecular modeling revealed that mutations in the histone core likely affect nucleosome stability, while the mutations in the tail affect various protein-protein interactions. In addition to molecular modeling data, previous work in other species such as yeast can provide insights

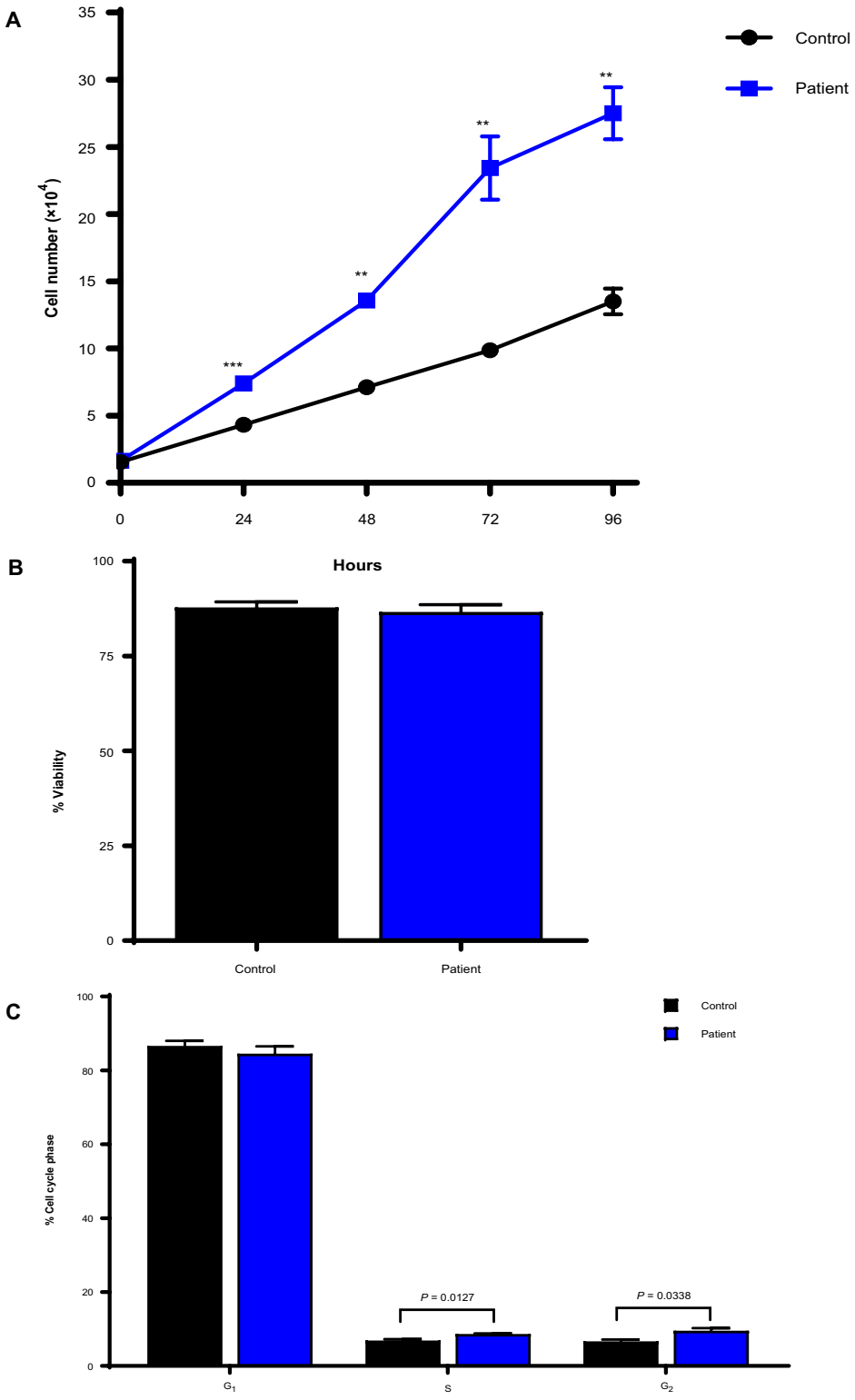

Fig. 5. Cellular dynamics of patient fibroblasts. (**A**) Five *H3F3A/B* patient fibroblast lines (*H3F3B*: p.G34V; *H3F3A*: p.R17G; *H3F3A*: p.G90R; *H3F3A*: p.T45I; and *H3F3B*: p.V117V or p.S146X in alternate transcript) demonstrated increased proliferation over six matched controls. $^{**}P < 0.005$ and $^{***}P < 0.0005$. Data represent means ± SEM of three biological replicates using three technical replicates each. (**B**) The same five *H3F3A/B* patient fibroblasts and six controls show no major differences in cell viability. The data represent the means ± SEM of four biological replicates using two technical replicates each. (**C**) Cell cycle analysis showed differences in the S ($P = 0.0127$) and G_2 ($P = 0.0338$) phase in the same five patient cell line compared to the six control fibroblast lines. Data represent the means ± SEM of four biological replicates using two technical replicates each.

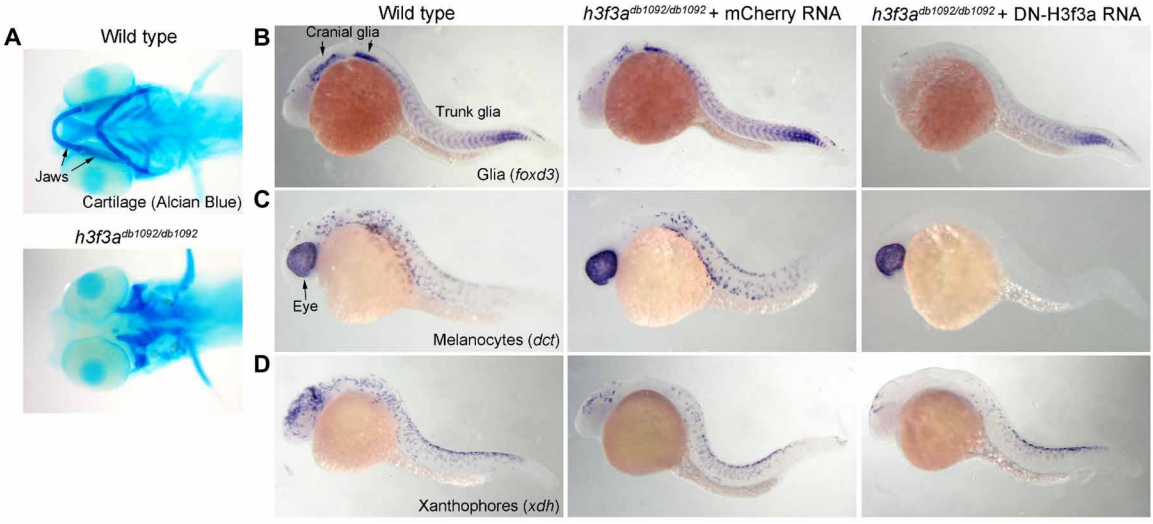

Fig. 6. Requirement of H3.3A for neural crest–derived glia and pigment cells. (**A**) Ventral whole-mount views of larval zebrafish heads at 5 dpf stained with Alcian Blue. Homozygous *h3f3a*^{db1092} mutants display complete loss of neural crest–derived jaw cartilages ($n = 10/10$). (**B** to **D**) In situ hybridization of zebrafish embryos for markers of glia (*foxd3*; 24 hpf), melanocytes (*dct*; 27 hpf), and xanthophores (*xdh*; 27 hpf). Homozygous *h3f3a*^{db1092} mutants injected at the one-cell stage with a control mCherry RNA show partial reductions in cranial glia ($n = 5$), melanocytes ($n = 4$), and xanthophores ($n = 3$), while those injected with dominant-negative H3f3a RNA to further reduced H3.3A function show complete loss of melanocytes ($n = 5$) and severe reductions of glia ($n = 6$) and xanthophores ($n = 4$) throughout cranial and trunk regions.

into the pathogenic mechanism of these variants. Of particular interest, two of the five amino acids that differentiate H3.3 from canonical H3 (p.S31 and p.G90) are mutated in our patient cohort. Both p.S31 and p.G90 are essential for proper recognition of H3.3 by other proteins. Mutagenic analysis in yeast shows that mutations at p.G90 prevent H3.3-specific chaperones DAXX and UBN1 (Ubinuclein 1) from binding (*20*). The serine at position 31 is required for recognition of H3.3 by ZMYND11 (*21*). Mutations in ZMYND11 cause an autosomal dominant neurodevelopmental phenotype similar to that seen in our patient cohort, including hypotonia, seizures, dysmorphic facial features, and developmental delay (*22*). A second mutation in our patient cohort, p.G34V, has also been shown to disrupt ZMYND11 binding to H3.3 (*21*). Other variants may disrupt histone octamer formation, nucleosome sliding, and chaperone binding based on mutagenic analysis of both H3 and H3.3 in model organisms (*23*–*25*). We hypothesized that additional missense mutations in our cohort induce epigenetic dysregulation of histone PTMs. These histones' PTMs within the nucleosome affect chromatin state, mitotic initiation, protein-chromatin interactions, and gene expression (*26*–*30*). Specific PTMs of unincorporated histones also mediate chaperone recognition before incorporation into the nucleosome (*31*).

The fact that all of these mutations are heterozygous is particularly noteworthy. Since there are two genes that produce H3.3, a heterozygous mutation in one of them means that 75% of the alleles are WT. A missense mutation in only 25% of the alleles is sufficient to cause global developmental delay, hypomyelination, cortical atrophy, and craniofacial anomalies. *H3F3A* and *H3F3B* are not expressed at the same levels so the amount of mutant protein could be more or less than 25% in any individual patient or tissue at any particular time; however, we observe the same phenotype regardless of whether the mutation is in *H3F3A* or *H3F3B* so a higher expression level from one of the genes cannot explain the severity of the phenotype. The fact that a single missense mutation in one allele causes such a severe phenotype strongly supports the importance of tight regulation of histones and histone PTMs. Furthermore, since our studies showed that the changes in the PTMs are in cis on the mutant H3.3 and not in trans on the WT H3.3 in the same nucleosome as is observed in the cancer causing mutations, the severity of the phenotype cannot be explained by a global dysregulation of PTMs.

Although the exact mechanism of the cellular pathology in these patients is unclear, H3.3 is vital for normal neurologic functioning. A recent study showed that H3.3 begins to replace H3.1 and H3.2 in postnatal mouse and human brains in a time-dependent manner and displaces these canonical H3 variants almost completely in adulthood. The important role of H3.3 over time may explain the unique neurodegenerative phenotype, as mice with decreased H3.3 expression in the hippocampus have impaired long-term memory (*32*). Humans with major depressive disorder have increased percentages of H3.3 in the nucleus accumbens, which is modulated by antidepressant therapy (*33*). This suggests that H3.3 modulators may represent potential targeted therapies for H3.3-related disorders and perhaps associated neuropsychiatric conditions in the general population. Future studies in patient-derived induced pluripotent stem cell neural cell types may further elucidate the underlying pathology.

Although these are the first germline variants associated with histone H3, germline variants in histones H1 and H4 with similar features have been reported. The overgrowth and neurodevelopmental delay associated with Rahman syndrome (MIM 617537) are caused by truncating variants in H1 Histone Family, Member E (*HIST1H1E*). (*34*) Recently, two specific germline variants in histone H4, which caused delayed growth and neurodevelopment, have been described in two families (*35*). In addition, there are many neurodevelopmental disorders associated with the histone lysine methylases and demethylases. These histone-related disorders provide a unique window into the role of histones in the control of development and growth.

In conclusion, we show here that heterozygous de novo missense variants in *H3F3A* and *H3F3B*, coding for H3.3, are associated with a previously undescribed phenotype of developmental delay,

neurodegeneration, epilepsy, facial dysmorphism, and congenital anomalies. The functional effects of these mutations appear to be different from those that are well-studied in cancer and may offer a target for therapy for these and other patients.

MATERIALS AND METHODS

The Institutional Review Boards of Columbia University, the University of Michigan, Children's Hospital of Eastern Ontario, University Medical Center Hamburg-Eppendorf, and the Children's Hospital of Philadelphia approved this study. Informed consent was obtained from all individual participants included in the study. Additional informed consent was obtained from all individual participants for whom identifying information is included in this article.

Exome and genome sequencing

Genomic DNA was extracted from whole blood from the affected children and their parents. Exome or genome sequencing was performed with a variety of standard capture kits and the general assertion criteria for variant classification following ACMGG/AMP (American College of Medical Genetics and Genomics/Association for Molecular Pathology) guidelines (*36*). There were no other variants in these patients that survived filtration and analysis using either dominant or recessive models and could explain the phenotypes.

Patient and control fibroblast cell lines

Six healthy control cells lines that were matched to available patient cells for passage number, age, and sex were obtained from the Coriell Institute for Medical Research tissue bank. All these fibroblast samples were derived from skin biopsies performed either on the arm or on the leg of the patient. Only a portion of the patients who participated in our study agreed to donate cellular material, and the patient mutations that were analyzed reflect the sum of the viable donations.

Histone derivatization and PTM analysis by nano–LC-MS

Histones were purified in acid as previously described by Karch *et al.* (*37*). Acid-extracted histones (15 to 25 μg) were resuspended in 100 mM ammonium bicarbonate (pH 8), derivatized using propionic anhydride, and digested with trypsin as previously described (*37*). The resulting histone peptides were desalted using the C18 Stage Tips, dried using a centrifugal evaporator, and reconstituted using 0.1% formic acid in preparation for nano–LC-MS analysis.

Nano-LC was performed using the Thermo Fisher Scientific Easy nLC 1000 System equipped with a 75 μm by 20 cm in-house packed column using Reprosil-Pur C18-AQ (3 μm; Maisch GmbH, Germany). Buffer A was 0.1% formic acid, and buffer B was 0.1% formic acid in 100% acetonitrile. Peptides were resolved using a two-step gradient from 0 to 26% B over 45 min and then from 26 to 98% B over 10 min at a flow rate of 300 nl/min. The high-performance LC was coupled online to an Orbitrap Elite mass spectrometer operating in the positive mode using a Nanospray Flex ion source (Thermo Fisher Scientific) at 2.40 kV. MS was performed using data-independent acquisition (DIA) as previously described with slight modifications (*37*). Briefly, two full MS scans [mass/charge ratio (m/z), 300 to 100) were acquired in the Orbitrap with a resolution of 120,000 (at 200 m/z) every eight DIA MS/MS events using isolation windows of 50 m/z each (e.g., 300 to 350, 350 to 400… 650 to 700). The full MS scan is performed twice within the same duty cycle to allow for a more resolved definition of the precursor peak profile. MS/MS events were acquired in the ion trap operating in normal mode. Fragmentation was performed using collision-induced dissociation in the ion trap mass analyzer with a normalized collision energy of 35. Automatic gain control (AGC) target and maximum injection time were 10×10^6 and 50 ms for the full MS scan and 10×10^4 and 150 ms for the MS/MS scan, respectively.

Data were searched using EpiProfile. The peptide relative ratio was calculated using the total area under the extracted ion chromatograms of all peptides with the same amino acid sequence (including all of its modified forms) as 100%. For isobaric peptides, the relative ratio of two isobaric forms was estimated by averaging the ratio for each fragment ion with different mass between the two species. Two to three biological replicates were analyzed per condition, and the relative abundance of each peptide modification was averaged across the runs.

Western blot validations

Isolated histones were separated on a 4 to 12% NuPAGE bis-tris gel and transferred to a 0.2-μm nitrocellulose blotting membrane. Membranes were blocked in TBS-T [50 mM tris-HCl (pH 7.5), 150 mM NaCl, and 0.1% Tween 20] containing 5% milk powder and probed for H3.3 (Thermo Fisher Scientific, MA5-24667; 1:5000), H3 (Abcam, ab1791; 1:5000), and H4 (Abcam, ab7311; 1:5000) primary antibodies diluted in TBS-T containing 5% milk powder. This was followed by anti-rabbit horseradish peroxidase (Abcam, ab99697; 1:10,000) and visualized using enhanced chemiluminesence prime Western blotting detection chemiluminescent reagent.

RNA-seq expression analysis

RNA was extracted using the RNeasy Mini Kit (QIAGEN) on the six samples at the same time. Extracted RNA samples underwent quality control assessment using Bioanalyzer (Agilent, Santa Clara, CA, USA) and were quantified using NanoDrop from NanoDrop Technologies (Wilmington, DE, USA). RNA libraries were prepared using the Illumina TruSeq RNA sample prep V2 with ribosomal RNA depletion and were sequenced using HiSeq 2500 sequencer (Illumina Inc., San Diego, CA, USA) at the Center for Applied Genomics at the Children's Hospital of Philadelphia per standard protocols (paired-end 100 base pairs). The RNA-seq data were aligned on the hg19 reference genome using STAR (www.encodeproject.org/software/star/) and processed using Cufflinks (http://cole-trapnell-lab.github.io/cufflinks/). For each gene, we compared the expression levels between cases and controls. A gene was considered differentially expressed if the P value is less than 0.05 and fragments per kilobase of transcript per million mapped reads has at least twofold change. To identify overrepresented functional categories among genes that are differentially expressed, we performed annotation analysis using the David Functional Annotation Resource (https://david.ncifcrf.gov/). Multiple testing was adjusted using the Benjamini-Hochberg approach, and enrichment was declared if the adjusted P value is less than 0.05.

Cellular analysis

Cellular proliferation was assayed with five patients and six control fibroblast cell lines; they were plated at 3×10^4 cells per well and then were manually counted at baseline, 24, 48, 72, and 96 hours. Then, the means ± SEM of three biological replicates using three technical replicates each were analyzed. Cell viability was analyzed with three patients and three control fibroblast cell lines; the cells were plated and grown until ~80% confluent. Then, they were stained for annexin V/propidium iodide (PI), and fluorescence-activated cell

sorting (FACS) was performed on Accuri C6 (BD Biosciences). Then, the means ± SEM of four biological replicates using two technical replicates each were analyzed. Cell cycle analysis was performed with three patients and three control fibroblast cell lines; the cells were plated and grown until ~80% confluent. They were then stained for PI, and FACS was performed on Calibur and analyzed by FlowJo. Then, the means ± SEM of four biological replicates using two technical replicates each were analyzed.

Zebrafish analysis

All zebrafish experiments were approved by the University of Southern California Institutional Animal Care and Use Committee (protocol #20258). *h3f3a*^{db1092} mutants were genotyped, and control mCherry or dominant-negative D123N H3f3a mRNAs were prepared and injected at 900 ng/μl into one-cell stage embryos as described (*18*). Acid-free cartilage staining with Alcian Blue was performed as described (*38*). In situ hybridization was performed with the probes and procedures described in (*18*). Images were captured on a Leica DM2500 compound microscope.

Computational analysis of structural location of the variants

For each H3.3 variant location, we analyzed its pattern of interatomic contacts (see below) using experimental structural information. The list of known structures was retrieved from the UniProt record of H3.3 (P84243). In all cases, the structure of H3.3 was incomplete, that is, only a fragment in complex with other proteins is described. For each variant, we identified the Protein Data Bank (PDB) entries that provided information about its location. We provide a table of the PDB files used in table S5.

Computing interactions at the native locus

For each variant, we computed the network of interatomic interactions of the native residue. This network was obtained following a simple protocol: (i) retrieve the corresponding PDB, (ii) compute the network of interactions for all the protein residues using Ring, (iii) extract the interaction data corresponding to the native residue, and (iv) organize these interaction data into three groups [intramonomer (within the same H3.3 monomer), intermonomer (between H3.3 monomer and other proteins), and H3.3-DNA] (*39*). Intramonomer interactions were only kept when the atoms involved came from residue pairs (i,j) separated by more than two residues in sequence, i.e., $|i - j| > 2$. Ring computations were executed with default parameters, except for "interaction type," which was set to "all." H3.3-DNA contacts were only included if their distance was lower than 5.5 Å.

SUPPLEMENTARY MATERIALS

Supplementary material for this article is available at http://advances.sciencemag.org/cgi/content/full/6/49/eabc9207/DC1

View/request a protocol for this paper from *Bio-protocol*.

REFERENCES AND NOTES

1. Z. Zhao, A. Shilatifard, Epigenetic modifications of histones in cancer. *Genome Biol.* **20**, 245 (2019).
2. J. H. Kim, J. H. Lee, I. S. Lee, S. B. Lee, K. S. Cho, Histone lysine methylation and neurodevelopmental disorders. *Int. J. Mol. Sci.* **18**, 1404 (2017).
3. C. J. Peter, S. Akbarian, Balancing histone methylation activities in psychiatric disorders. *Trends Mol. Med.* **17**, 372–379 (2011).
4. R. A. Bagchi, K. L. Weeks, Histone deacetylases in cardiovascular and metabolic diseases. *J. Mol. Cell. Cardiol.* **130**, 151–159 (2019).
5. R. N. Wickramasekara, H. A. F. Stessman, Histone 4 lysine 20 methylation: A case for neurodevelopmental disease. *Biology* **8**, 11 (2019).
6. J. Schwartzentruber, A. Korshunov, X. Y. Liu, D. T. Jones, E. Pfaff, K. Jacob, D. Sturm, A. M. Fontebasso, D. A. Quang, M. Tonjes, V. Hovestadt, S. Albrecht, M. Kool, A. Nantel, C. Konermann, A. Lindroth, N. Jager, T. Rausch, M. Ryzhova, J. O. Korbel, T. Hielscher, P. Hauser, M. Garami, A. Klekner, L. Bognar, M. Ebinger, M. U. Schuhmann, W. Scheurlen, A. Pekrun, M. C. Fruhwald, W. Roggendorf, C. Kramm, M. Durken, J. Atkinson, P. Lepage, A. Montpetit, M. Zakrzewska, K. Zakrzewski, P. P. Liberski, Z. Dong, P. Siegel, A. E. Kulozik, M. Zapatka, A. Guha, D. Malkin, J. Felsberg, G. Reifenberger, A. von Deimling, K. Ichimura, V. P. Collins, H. Witt, T. Milde, O. Witt, C. Zhang, P. Castelo-Branco, P. Lichter, D. Faury, U. Tabori, C. Plass, J. Majewski, S. M. Pfister, N. Jabado, Driver mutations in histone H3.3 and chromatin remodelling genes in paediatric glioblastoma. *Nature* **482**, 226–231 (2012).
7. A. Maver, G. Cuturilo, S. J. Ruml, B. Peterlin, Clinical next generation sequencing reveals an H3F3A gene as a new potential gene candidate for microcephaly associated with severe developmental delay, intellectual disability and growth retardation. *Balkan J. Med. Genet.* **22**, 65–68 (2019).
8. T. H. Ederveen, I. K. Mandemaker, C. Logie, The human histone H3 complement anno 2011. *Biochim. Biophys. Acta* **1809**, 577–586 (2011).
9. C. W. Jang, Y. Shibata, J. Starmer, D. Yee, T. Magnuson, Histone H3.3 maintains genome integrity during mammalian development. *Genes Dev.* **29**, 1377–1392 (2015).
10. K. M. Bush, B. T. Yuen, B. L. Barrilleaux, J. W. Riggs, H. O'Geen, R. F. Cotterman, P. S. Knoepfler, Endogenous mammalian histone H3.3 exhibits chromatin-related functions during development. *Epigenetics Chromatin* **6**, 7 (2013).
11. A. Sakai, B. E. Schwartz, S. Goldstein, K. Ahmad, Transcriptional and developmental functions of the H3.3 histone variant in Drosophila. *Curr. Biol.* **19**, 1816–1820 (2009).
12. K. K. Lim, T. Y. Ong, Y. R. Tan, E. G. Yang, B. Ren, K. S. Seah, Z. Yang, T. S. Tan, B. W. Dymock, E. S. Chen, Mutation of histone H3 serine 86 disrupts GATA factor Ams2 expression and precise chromosome segregation in fission yeast. *Sci. Rep.* **5**, 14064 (2015).
13. M. Lek, K. J. Karczewski, E. V. Minikel, K. E. Samocha, E. Banks, T. Fennell, A. H. O'Donnell-Luria, J. S. Ware, A. J. Hill, B. B. Cummings, T. Tukiainen, D. P. Birnbaum, J. A. Kosmicki, L. E. Duncan, K. Estrada, F. Zhao, J. Zou, E. Pierce-Hoffman, J. Berghout, D. N. Cooper, N. Deflaux, M. DePristo, R. Do, J. Flannick, M. Fromer, L. Gauthier, J. Goldstein, N. Gupta, D. Howrigan, A. Kiezun, M. I. Kurki, A. L. Moonshine, P. Natarajan, L. Orozco, G. M. Peloso, R. Poplin, M. A. Rivas, V. Ruano-Rubio, S. A. Rose, D. M. Ruderfer, K. Shakir, P. D. Stenson, C. Stevens, B. P. Thomas, G. Tiao, M. T. Tusie-Luna, B. Weisburd, H. H. Won, D. Yu, D. M. Altshuler, D. Ardissino, M. Boehnke, J. Danesh, S. Donnelly, R. Elosua, J. C. Florez, S. B. Gabriel, G. Getz, S. J. Glatt, C. M. Hultman, S. Kathiresan, M. Laakso, S. McCarroll, M. I. McCarthy, D. McGovern, R. McPherson, B. M. Neale, A. Palotie, S. M. Purcell, D. Saleheen, J. M. Scharf, P. Sklar, P. F. Sullivan, J. Tuomilehto, M. T. Tsuang, H. C. Watkins, J. G. Wilson, M. J. Daly, D. G. MacArthur; C. Exome Aggregation, Analysis of protein-coding genetic variation in 60,706 humans. *Nature* **536**, 285–291 (2016).
14. S. Pepenella, K. J. Murphy, J. J. Hayes, Intra- and inter-nucleosome interactions of the core histone tail domains in higher-order chromatin structure. *Chromosoma* **123**, 3–13 (2014).
15. S. Sidoli, B. A. Garcia, Properly reading the histone code by MS-based proteomics. *Proteomics* **15**, 2901–2902 (2015).
16. S. Papillon-Cavanagh, C. Lu, T. Gayden, L. G. Mikael, D. Bechet, C. Karamboulas, L. Ailles, J. Karamchandani, D. M. Marchione, B. A. Garcia, I. Weinreb, D. Goldstein, P. W. Lewis, O. M. Dancu, S. Dhaliwal, W. Stecho, C. J. Howlett, J. S. Mymryk, J. W. Barrett, A. C. Nichols, C. D. Allis, J. Majewski, N. Jabado, Impaired H3K36 methylation defines a subset of head and neck squamous cell carcinomas. *Nat. Genet.* **49**, 180–185 (2017).
17. P. W. Lewis, M. M. Muller, M. S. Koletsky, F. Cordero, S. Lin, L. A. Banaszynski, B. A. Garcia, T. W. Muir, O. J. Becher, C. D. Allis, Inhibition of PRC2 activity by a gain-of-function H3 mutation found in pediatric glioblastoma. *Science* **340**, 857–861 (2013).
18. S. G. Cox, H. Kim, A. T. Garnett, D. M. Medeiros, W. An, J. G. Crump, An essential role of variant histone H3.3 for ectomesenchyme potential of the cranial neural crest. *PLOS Genet.* **8**, e1002938 (2012).
19. B. R. Lowe, L. A. Maxham, J. J. Hamey, M. R. Wilkins, J. F. Partridge, Histone H3 mutations: An updated view of their role in chromatin deregulation and cancer. *Cancers* **11**, 660 (2019).
20. M. D. Ricketts, B. Frederick, H. Hoff, Y. Tang, D. C. Schultz, T. Singh Rai, M. Grazia Vizioli, P. D. Adams, R. Marmorstein, Ubinuclein-1 confers histone H3.3-specific-binding by the HIRA histone chaperone complex. *Nat. Commun.* **6**, 7711 (2015).
21. H. Wen, Y. Li, Y. Xi, S. Jiang, S. Stratton, D. Peng, K. Tanaka, Y. Ren, Z. Xia, J. Wu, B. Li, M. C. Barton, W. Li, H. Li, X. Shi, ZMYND11 links histone H3.3K36me3 to transcription elongation and tumour suppression. *Nature* **508**, 263–268 (2014).
22. A. M. Moskowitz, N. Belnap, A. L. Siniard, S. Szelinger, A. M. Claasen, R. F. Richholt, M. De Both, J. J. Corneveaux, C. Balak, I. S. Piras, M. Russell, A. L. Courtright, S. Rangasamy, K. Ramsey, D. W. Craig, V. Narayanan, M. J. Huentelman, I. Schrauwen, A de novo missense mutation in ZMYND11 is associated with global developmental delay, seizures, and hypotonia. *Cold Spring Harb. Mol. Case Stud.* **2**, a000851 (2016).
23. P. Johnson, V. Mitchell, K. McClure, M. Kellems, S. Marshall, M. K. Allison, H. Lindley, H. T. Nguyen, J. E. Tackett, A. A. Duina, A systematic mutational analysis of a histone H3

residue in budding yeast provides insights into chromatin dynamics. *G3* **5**, 741–749 (2015).
24. A. Norris, M. A. Bianchet, J. D. Boeke, Compensatory interactions between Sir3p and the nucleosomal LRS surface imply their direct interaction. *PLOS Genet.* **4**, e1000301 (2008).
25. K. Matsubara, N. Sano, T. Umehara, M. Horikoshi, Global analysis of functional surfaces of core histones with comprehensive point mutants. *Genes Cells* **12**, 13–33 (2007).
26. S. B. Hake, C. D. Allis, Histone H3 variants and their potential role in indexing mammalian genomes: The "H3 barcode hypothesis". *Proc. Natl. Acad. Sci. U.S.A.* **103**, 6428–6435 (2006).
27. A. Schulmeister, M. Schmid, E. M. Thompson, Phosphorylation of the histone H3.3 variant in mitosis and meiosis of the urochordate Oikopleura dioica. *Chromosome Res.* **15**, 189–201 (2007).
28. P. N. Lau, P. Cheung, Histone code pathway involving H3 S28 phosphorylation and K27 acetylation activates transcription and antagonizes polycomb silencing. *Proc. Natl. Acad. Sci. U.S.A.* **108**, 2801–2806 (2011).
29. A. Sawicka, C. Seiser, Histone H3 phosphorylation—A versatile chromatin modification for different occasions. *Biochimie* **94**, 2193–2201 (2012).
30. F. T. Chang, F. L. Chan, J. D. R. McGhie, M. Udugama, L. Mayne, P. Collas, J. R. Mann, L. H. Wong, CHK1-driven histone H3.3 serine 31 phosphorylation is important for chromatin maintenance and cell survival in human ALT cancer cells. *Nucleic Acids Res.* **43**, 2603–2614 (2015).
31. R. J. Burgess, Z. Zhang, Histone chaperones in nucleosome assembly and human disease. *Nat. Struct. Mol. Biol.* **20**, 14–22 (2013).
32. I. Maze, W. Wenderski, K. M. Noh, R. C. Bagot, N. Tzavaras, I. Purushothaman, S. J. Elsasser, Y. Guo, C. Ionete, Y. L. Hurd, C. A. Tamminga, T. Halene, L. Farrelly, A. A. Soshnev, D. Wen, S. Rafii, M. R. Birtwistle, S. Akbarian, B. A. Buchholz, R. D. Blitzer, E. J. Nestler, Z. F. Yuan, B. A. Garcia, L. Shen, H. Molina, C. D. Allis, Critical role of histone turnover in neuronal transcription and plasticity. *Neuron* **87**, 77–94 (2015).
33. A. E. Lepack, R. C. Bagot, C. J. Pena, Y. E. Loh, L. A. Farrelly, Y. Lu, S. K. Powell, Z. S. Lorsch, O. Issler, H. M. Cates, C. A. Tamminga, H. Molina, L. Shen, E. J. Nestler, C. D. Allis, I. Maze, Aberrant H3.3 dynamics in NAc promote vulnerability to depressive-like behavior. *Proc. Natl. Acad. Sci. U.S.A.* **113**, 12562–12567 (2016).
34. K. Tatton-Brown, C. Loveday, S. Yost, M. Clarke, E. Ramsay, A. Zachariou, A. Elliott, H. Wylie, A. Ardissone, O. Rittinger, F. Stewart, I. K. Temple, T. Cole, C. Childhood Overgrowth, S. Mahamdallie, S. Seal, E. Ruark, N. Rahman, Mutations in epigenetic regulation genes are a major cause of overgrowth with intellectual disability. *Am. J. Hum. Genet.* **100**, 725–736 (2017).
35. F. Tessadori, J. C. Giltay, J. A. Hurst, M. P. Massink, K. Duran, H. R. Vos, R. M. van Es; Deciphering Developmental Disorders Study, R. H. Scott, K. L. I. van Gassen, J. Bakkers, G. van Haaften, Germline mutations affecting the histone H4 core cause a developmental syndrome by altering DNA damage response and cell cycle control. *Nat. Genet.* **49**, 1642–1646 (2017).
36. S. Richards, N. Aziz, S. Bale, D. Bick, S. Das, J. Gastier-Foster, W. W. Grody, M. Hegde, E. Lyon, E. Spector, K. Voelkerding, H. L. Rehm; ACMG Laboratory Quality Assurance Committee, Standards and guidelines for the interpretation of sequence variants: A joint consensus recommendation of the American College of Medical Genetics and Genomics and the Association for Molecular Pathology. *Genet. Med.* **17**, 405–423 (2015).
37. K. R. Karch, S. Sidoli, B. A. Garcia, Identification and quantification of histone PTMs using high-resolution mass spectrometry. *Methods Enzymol.* **574**, 3–29 (2016).
38. M. B. Walker, C. B. Kimmel, A two-color acid-free cartilage and bone stain for zebrafish larvae. *Biotech. Histochem.* **82**, 23–28 (2007).
39. D. Piovesan, G. Minervini, S. C. Tosatto, The RING 2.0 web server for high quality residue interaction networks. *Nucleic Acids Res.* **44**, W367–W374 (2016).

Acknowledgments: We thank the families for contribution. We also thank J. F. Deleuze, A. Boland, and V. Meyer from the CNRGH for genome sequencing and data primary analysis. **Funding:** Funding was provided by the French Foundation for Rare Diseases (Fondation maladies rares). This work was also supported in part by a grant from the from SFARI (to W.K.C.), JPB Foundation (to W.K.C.), and the Morton S. and Henrietta K. Sellner Professorship in Human Genetics (to J.W.I.), as well as an NIDDK T35 training grant (T35DK093430) (to E.F.J.). E.J.B. was supported by a K12 training grant (K12HD043245-14) and the Roberts Collaborative. D.M. was supported by a T32 training grant (T32GM008275). Funding from NIH grants GM110174 and CA196539 to B.G. is acknowledged. This research was funded in part by the Estonian Science Foundation grant PUT0355 and PRG471. Analysis for one patient was provided by the Broad Institute of MIT and Harvard Center for Mendelian Genomics (Broad CMG) and was funded by the National Human Genome Research Institute, the National Eye Institute, and the National Heart, Lung, and Blood Institute grant UM1 HG008900 to D. MacArthur and H. Rehm. Support also provided by NIH T32 HD07466 (to M.H.W.), Alabama Genomic Health Initiative F170303004 through University of Alabama at Birmingham IRB (to A.C.H., J.D., and M.T.) The Toronto-based authors (to G.C., M.S.M., and D.C.) acknowledge support from the Centre for Genetic Medicine, The Centre for Applied Genomics, and the Norman Saunders Complex Care Initiative. The Care4Rare Canada Consortium is funded by Genome Canada, the Canadian Institutes of Health Research, the Ontario Genomics Institute, Ontario Research Fund, Genome Quebec, and Children's Hospital of Eastern Ontario Foundation. This work was also supported by Dipartimenti di Eccellenza 2018–2022 Project code D15D18000410001 to A.B. and Fondazione Bambino Gesù (Vite Coraggiose) and Italian Ministry of Health (CCR-2017-23669081) to M.T. **Author contributions:** A.B., A.C.H., A.J.Y., A.L., A.P.A.S., A.Z., B.F., C.F., C.G.S.P., C.T.R.M.S., D.H., D.N., E.Bri., E.Bro., E.V., F.C.R., H.K., G.B.F., G.G., J.A.M.-A., J.C.P., J.M.T., J.Ne., J.No., J.S.S., K.E.S., K.M., K.T., K.Wie., K.Wil., L.B., L.U., L.W.L., M.B., M.G.M., M.I.V.A., M.S., M.Ta., M.Th., N.H.P., N.L., R.J.L., R.R.L., S.A.S.V., S.F.N., S.J.C.S., S.M.-A., S.S.C., T.H., T.P., W.K.C., E.J.B., M.J.Lyo., M.J.Lar., W.C., E.She., E.Sel., K.J.W., A.W., G.M.S.M., N.P.-H., J.v.d.K., T.G., John Dean, J.Den., Joy Dean, A.R., H.P.C., M.C.W., L.M., C.N., A.A., D.Les., T.K., J.Win., J.Wan., C.B.C., A.Vol., A.Van., E.F.J., J.L.S., J.W.I., A.P., S.L., H.D., J.H., H.R., B.K., O.S., S.O., S.M., K.Ret., K.Rad., K.Ö., P.I., A.M.I., G.C., M.S.M., D.Chi., D.Car., M.M.W., and E.Z. contributed to the clinical evaluation of the affected individuals. R.B., J.A.L., B.R., Z.P., M.C., R.S., D.Les., M.W., K.Ret., K.Rad., T.M.S., K.G.M., R.G., K.R., C.M., K.L.H., B.C., S.Bez., S.Bar., T.B., S.K., R.R., M.H.W., K.D.K., Care4Rare Canada Consortium, CAUSES Study, DDD Study, and Undiagnosed Disease Program contributed to the molecular evaluation of the affected individuals. E.J.B., D.Les., H.H.H., M.E.M., B.G., D.M., K.J., Z.-F.Y., P.L., C.S., J.G.C., X.d.l.C., N.P., S.G.C., K.Wil., and D.Li contributed the functional evaluation of the variants found in the affected individuals. **Competing interests:** K.R. and K.M. are employees of GeneDx. W.K.C. and M.C. were employees of GeneDx. The authors declare that they have no other competing interests. **Data and materials availability:** Patient variants will be available in ClinVar. All patient materials may be obtained through a material transfer agreement. All other data needed to evaluate the conclusions in the paper are present in the paper and/or the Supplementary Materials. Additional data related to this paper may be requested from the authors.

Submitted 21 May 2020
Accepted 19 October 2020
Published 2 December 2020
10.1126/sciadv.abc9207

Citation: L. Bryant, D. Li, S. G. Cox, D. Marchione, E. F. Joiner, K. Wilson, K. Janssen, P. Lee, M. E. March, D. Nair, E. Sherr, B. Fregeau, K. J. Wierenga, A. Wadley, G. M. S. Mancini, N. Powell-Hamilton, J. van de Kamp, T. Grebe, J. Dean, A. Ross, H. P. Crawford, Z. Powis, M. Cho, M. C. Willing, L. Manwaring, R. Schot, C. Nava, A. Afenjar, D. Lessel, M. Wagner, T. Klopstock, J. Winkelmann, C. B. Catarino, K. Retterer, J. L. Schuette, J. W. Innis, A. Pizzino, S. Lüttgen, J. Denecke, T. M. Strom, K. G. Monaghan; DDD Study, Z.-F. Yuan, H. Dubbs, R. Bend, J. A. Lee, M. J. Lyons, J. Hoefele, R. Günthner, H. Reutter, B. Keren, K. Radtke, O. Sherbini, C. Mrokse, K. L. Helbig, S. Odent, B. Cogne, S. Mercier, S. Bezieau, T. Besnard, S. Kury, R. Redon, K. Reinson, M. H. Wojcik, K. Õunap, P. Ilves, A. M. Innes, K. D. Kernohan; Care4Rare Canada Consortium, G. Costain, M. S. Meyn, D. Chitayat, E. Zackai, A. Lehman, H. Kitson; CAUSES Study, M. G. Martin, J. A. Martinez-Agosto, S. F. Nelson, C. G. S. Palmer, J. C. Papp, N. H. Parker, J. S. Sinsheimer, E. Vilain, J. Wan, A. J. Yoon, A. Zheng, E. Brimble, G. B. Ferrero, F. C. Radio, D. Carli, S. Barresi, A. Brusco, M. Tartaglia, J. M. Thomas, L. Umana, M. M. Weiss, G. Gotway, K. E. Stuurman, M. L. Thompson, K. McWalter, C. T. R. M. Stumpel, S. J. C. Stevens, A. P. A. Stegmann, K. Tveten, A. Vøllo, T. Prescott, C. Fagerberg, L. W. Laulund, M. J. Larsen, M. Byler, R. R. Lebel, A. C. Hurst, J. Dean, S. A. Schrier Vergano, J. Norman, S. Mercimek-Andrews, J. Neira, M. I. Van Allen, N. Longo, E. Sellars, R. J. Louie, S. S. Cathey, E. Brokamp, D. Heron, M. Snyder, A. Vanderver, C. Simon, X. de la Cruz, N. Padilla, J. G. Crump, W. K. Chung, B. Garcia, H. H. Hakonarson, E. J. Bhoj, Histone H3.3 beyond cancer: Germline mutations in *Histone 3 Family 3A and 3B* cause a previously unidentified neurodegenerative disorder in 46 patients. *Sci. Adv.* **6**, eabc9207 (2020).